

**Figure 4** Map of Jurassic continental configuration (modified from ref. 29) with cladogram showing relationships and provenance of known Jurassic caudates. The taxa at the tips of the cladogram are, from left to right: (1) *Marmorerpeton*; (2) *Karaurus* and *Kokartus*; (3) *Laccotriton* and *Sinerpeton*; (4) *Jeholotriton*; and (5) *Chunerpeton*. The dotted line indicates the uncertainty of the phylogenetic position of *Marmorerpeton*. The shaded area represents the extent of continents.

America represents a more recent dispersal, perhaps associated with the development of a land bridge<sup>19,20</sup>. Hynobiids, on the other hand, underwent a range contraction. As hynobiid fossils are known from the Miocene and Pleistocene of Europe<sup>23</sup>, this group probably extended its range out of Asia only to be limited to that continent by the Holocene epoch.

Despite its Bathonian age, the new cryptobranchid shows extraordinary morphological similarity to its living relatives. This similarity underscores the stasis within salamander anatomical evolution<sup>28</sup>. Indeed, extant cryptobranchid salamanders can be regarded as living fossils whose structures have remained little changed for over 160 million years. Furthermore, the new material from China reveals that the early diversification of salamanders was well underway by the Middle Jurassic; several extant taxa including hynobiids and cryptobranchids had already appeared by that time. Notably, this ancient pattern of taxonomic diversification does not correlate to any great disparity in anatomical structure. □

Received 19 December 2002; accepted 3 February 2003; doi:10.1038/nature01491.

1. Wake, D. B. & Larson, A. Multidimensional analysis of an evolving lineage. *Science* **238**, 42–48 (1987).
2. Wake, D. B. Homoplasy: the result of natural selection or evidence of design limitations? *Am. Nat.* **138**, 543–567 (1991).
3. Shubin, N., Wake, D. B. & Crawford, A. J. Morphological variation in the limbs of *Taricha granulosa* (Caudata: Salamandridae): evolutionary and phylogenetic implications. *Evolution* **49**, 874–884 (1995).
4. Shubin, N. & Wake, D. B. Phylogeny, variation, and morphological integration. *Am. Zool.* **36**, 51–60 (1996).
5. Gao, K.-Q. & Shubin, N. H. Late Jurassic salamanders from northern China. *Nature* **410**, 574–577 (2001).
6. Gao, K., Cheng, Z. & Xu, X. First report of Mesozoic urodeles from China. *Geol. China* **248**, 40–41 (1998).
7. Wang, Y. A new salamander (Amphibia: Caudata) from the Early Cretaceous Jehol Biota. *Vert. Palasiat.* **38**, 100–103 (2000).
8. Dong, Z. & Wang, Y. A new urodele (*Liaoxitriton zhongjiani* gen. et sp. nov.) from the Early Cretaceous of western Liaoning Province, China. *Vert. Palasiat.* **36**, 159–172 (1998).
9. Wang, S. et al. *Stratigraphical Lexicon of China: The Jurassic System* (Geological Publishing House, Beijing, 2000).
10. Krzeminski, W. & Ren, D. *Praemacrochile chinensis* n. sp. from the Middle Jurassic of China (Diptera: Tanyderidae). *Pol. Pis. Entomol.* **71**, 127–129 (2002).
11. Ren, D. & Oswald, J. D. A new genus of kalligrammatid lacewings from the Middle Jurassic of China (Neuroptera: Kalligrammatidae). *Stuttgart. Beit. Nat.* **33**, 1–8 (2002).
12. Ji, Q. & Yuan, C. Discovery of two kinds of protofeathered pterosaurs in the Mesozoic Daohugou Biota in the Ningcheng region and its stratigraphic and biologic significances. *Geol. Rev.* **48**, 221–224 (2002).
13. Ren, D. et al. On the biostratigraphy of the Jurassic fossil beds at Daohugou near Ningcheng, Inner Mongolia. *Geol. Bull. China* **21**, 584–591 (2002).
14. Naylor, B. G. Cryptobranchid salamanders from the Paleocene and Miocene of Saskatchewan. *Copeia* **1981**, 76–86 (1981).
15. Estes, R. *Handbuch der Paläoherpetologie Teil 2 Gymnophiona, Caudata* (Gustav Fischer, Stuttgart, 1981).
16. Gubin, Y. M. Paleocene salamanders from Southern Mongolia. *Paleontol. J.* **1991**, 91–102 (1991).
17. Harland, B. W. et al. *A Geologic Time Scale 1989* (Cambridge Univ. Press, Cambridge, 1990).
18. Evans, S. E. & Milner, A. R. A metamorphosed salamander from the Early Cretaceous of Las Hoyas, Spain. *Phil. Trans. R. Soc. Lond. B* **351**, 627–646 (1996).

19. Milner, A. R. in *Amphibian Biology* Vol. 4 (eds Heatwole, H. & Carroll, R. L.) 1412–1444 (Surrey Beatty, Chipping Norton, Australia, 2000).
20. Milner, A. R. in *Evolution, Time and Space: The Emergence of the Biosphere* (eds Sims, R. W., Price, J. H. & Whalley, P. E. S.) 431–468 (Academic, London, 1983).
21. Duellman, W. E. & Trueb, L. *Biology of Amphibians* (McGraw-Hill, New York, 1986).
22. Larson, A. & Dimmick, W. W. in *Amphibian Relationships: Phylogenetic Analysis of Morphology and Molecules* (eds Cannatella, D. & Hillis, D.). *Herpetol. Monogr.* **7**, 77–93 (1993).
23. Venczel, M. & Hír, J. in *Abstracts of the Third World Congress of Herpetology* (eds Roček, Z. & Hart, S.) 218–219, (Third World Congress of Herpetology, Prague, 1997).
24. Ivachnenko, M. F. Urodelans from the Triassic and Jurassic of Soviet Central Asia. *Paleontol. J.* **12**, 362–368 (1978).
25. Nesson, L. A. Late Mesozoic amphibians and lizards of Soviet Middle Asia. *Acta Zool. Cracov.* **31**, 475–486 (1988).
26. Nesson, L. A., Fedorov, P. V., Potanov, D. O. & Golovyeva, L. S. The structure of the skulls of caudate amphibians collected from the Jurassic of Kirgizstan and the Cretaceous of Uzbekistan. *Vest. Sankt-Peters. Univ. Geol.* **7**, 3–11 (1996).
27. Evans, S. E., Milner, A. R. & Mussett, F. The earliest known salamanders (Amphibia: Caudata): A record from the Middle Jurassic of England. *Geobios* **21**, 539–552 (1988).
28. Wake, D. B., Roth, G. & Wake, M. H. On the problem of stasis in organismal evolution. *J. Theor. Biol.* **101**, 211–224 (1983).
29. Scotese, C. R. *Atlas of Earth History* Vol. 1 *Paleogeography* (Paleomap Project, Arlington, Texas, 2001).

**Acknowledgements** We thank Q. Ji for providing access to the holotype specimen. M. Ellison did the photographs of the holotype; K. Monoyios performed the drawings. This research was supported by the National Science Foundation, the National Natural Science Foundation of China (K.-Q.G.), and a grant from the John Simon Guggenheim Memorial Foundation (N.S.).

**Competing interests statement** The authors declare that they have no competing financial interests.

**Correspondence** and requests for materials should be addressed to N.H.S. (e-mail: nshubin@uchicago.edu)

## Ecological and immunological determinants of influenza evolution

Neil M. Ferguson\*, Alison P. Galvani† & Robin M. Bush‡

\* Department of Infectious Disease Epidemiology, Faculty of Medicine, Imperial College London, St Mary's Campus, Norfolk Place, London W2 1PG, UK  
 † Department of Integrative Biology, University of California, Berkeley, California 94720-3140, USA  
 ‡ Department of Ecology and Evolutionary Biology, University of California, Irvine, 92697, USA

In pandemic and epidemic forms, influenza causes substantial, sometimes catastrophic, morbidity and mortality. Intense selection from the host immune system drives antigenic change in influenza A and B, resulting in continuous replacement of circulating strains with new variants able to re-infect hosts immune to earlier types. This 'antigenic drift'<sup>1</sup> often requires a new vaccine to be formulated before each annual epidemic. However, given the high transmissibility and mutation rate of influenza, the constancy of genetic diversity within lineages over time is paradoxical. Another enigma is the replacement of existing strains during a global pandemic caused by 'antigenic shift'—the introduction of a new avian influenza A subtype into the human population<sup>1</sup>. Here we explore ecological and immunological factors underlying these patterns using a mathematical model capturing both realistic epidemiological dynamics and viral evolution at the sequence level. By matching model output to phylogenetic patterns seen in sequence data collected through global surveillance<sup>2</sup>, we find that short-lived strain-transcending immunity is essential to restrict viral diversity in the host population and thus to explain key aspects of drift and shift dynamics.

The surface glycoprotein haemagglutinin of influenza is under strong selection by the human immune system as the primary antibody target<sup>2</sup>. Figure 1a–c shows phylogenies constructed using

the HA1 domain of the haemagglutinin gene of human influenza A subtypes H3N2 (H3) and H1N1 (H1), and for influenza B. The slender 'trunk' of the H3 tree characterizes the evolutionary pattern of antigenic drift, and reflects the serial replacement of strains. Although brief co-circulation of closely related H3 lineages is not uncommon<sup>3</sup>, the H3 tree appears to be linear because the average survival time of side lineages is only 1.6 years (ref. 4). The H1 tree is similar to that of H3, although recent bifurcation of the main trunk has resulted in several extant lineages. It remains to be seen whether more than one will persist. Influenza B exhibits greater branching than either A subtype, having diverged into two major lineages in the early 1970s and multiple minor lineages thereafter<sup>5</sup>.

The explanation for the variation in tree shape between influenza viruses, illustrated in Fig. 1, is unknown. Furthermore, different strains evolve at different rates (Fig. 1e). Most studies suggest that H3 changes more rapidly than H1, while influenza B evolves more slowly than either A subtype<sup>3</sup>. The fixation rates calculated for the H3, H1 and B trees in Fig. 1a–c are consistent with this, at 0.0037, 0.0018 and 0.0013 nucleotide substitutions per site per year ( $\pm 0.001$ ), respectively. However, providing a biological explanation for these differences is complicated by immunological interactions between subtypes and types (Fig. 1f), although some of the

variation may solely be a function of the short time periods studied<sup>6</sup> (here 14, 24 and 20 years for H3, H1 and B respectively).

Fixation rates averaged over the whole of HA1 obscure variation among codons. For instance, 35% of replacements occur at 18 (5.5%) of the 329 codons in HA1 of H3. The excess of non-synonymous versus synonymous substitutions at these 18 codons reflects intense positive selection<sup>2,7</sup>, possibly because these codons are associated with the receptor binding site or antibody binding sites on the HA1 surface. The contrast between the fixation rate of 0.053 ( $\pm 0.005$ ) substitutions per site per year in the tree of the 18 key codons alone (Fig. 1d), and a rate of 0.0015 ( $\pm 0.0001$ ) for the 311 other codons of H3 reveals the importance of small subsets of codons to influenza evolution. We focus on identifying immunological and ecological processes that shape selection at antigenically significant codons to result in the observed evolutionary patterns of antigenic drift.

The diversity of a pathogen population is determined by the balance between the production of new strains and the competition-induced stochastic extinction of existing variants. To explain the surprisingly limited genetic diversity of influenza, we use an individual-based simulation (see Methods) to explore four determinants of this balance: the generation of new variants through mutation or reassortment, the initial establishment of those variants

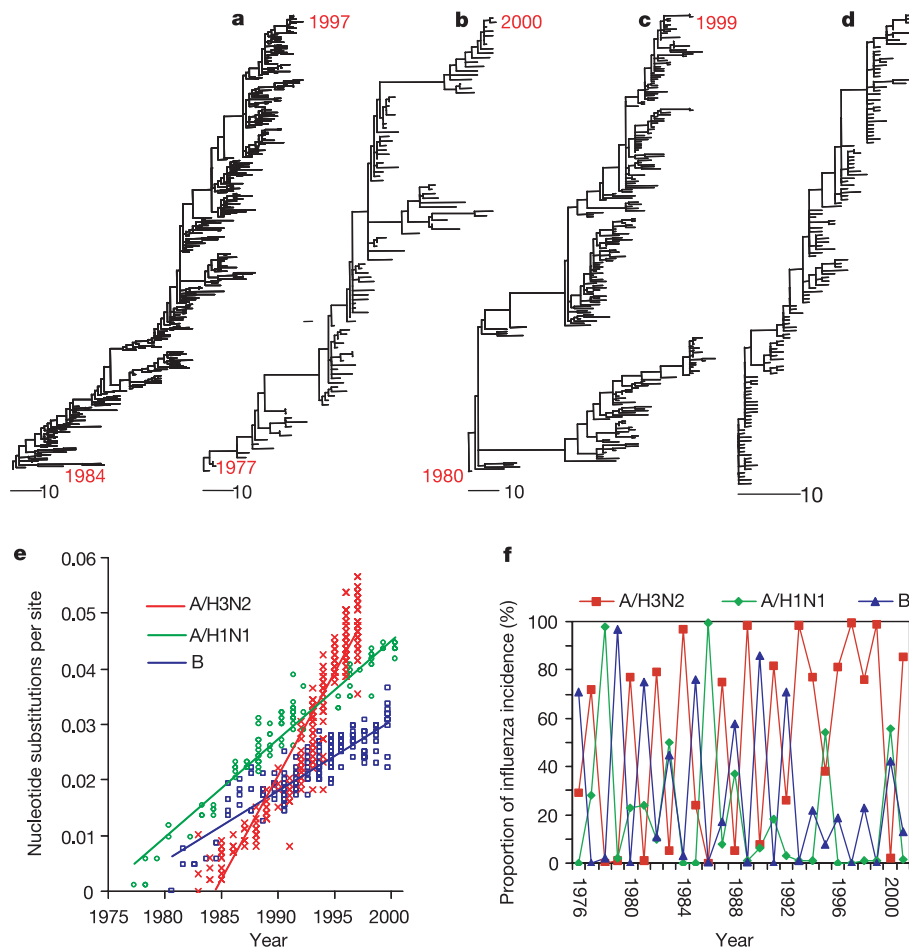


**Figure 1** Evolutionary dynamics of influenza. **a**, Evolution of human influenza A subtype H3 from 1983 to 1997 derived from 357 sequences of 987 nucleotides<sup>2</sup>. **b**, Influenza A subtype H1, derived using 104 sequences of 1,032 nucleotides collected between 1977 and 2000. **c**, Influenza B, derived from 220 sequences of 1,041 nucleotides collected between 1980 and 1999. **d**, As **a**, but with horizontal distance representing the number of substitutions at the 18 positively selected codons<sup>2</sup> and with zero-length branches removed. All trees were generated from HA1 sequences using the tree bisection-reconnection branch-swapping option of the heuristic search option of the maximum-

parsimony routine of PAUP<sup>29</sup>. Tree shape is robust to other phylogenetic algorithms. (See Supplementary Information for sequence data accession numbers.) **e**, Distance from the root of the tree to each terminal node in nucleotide substitutions against year of isolation. Slopes of lines illustrate differences in fixation rates between H3, H1 and B. **f**, Proportion of laboratory-analysed influenza infections isolates identified as H3, H1 or B each year by the World Health Organization laboratories in the United States from 1976 to 2001 (ref. 30). The trends shown are suggestive of interference between subtypes, with annually fluctuating subtype dominance.

in the host population, cross-immunity-mediated competition between strains, and the processes governing the rate of strain extinction. Although our model is computationally intensive, it captures realistic population genetics of large numbers of unique co-circulating strains, a simplified representation of the spatial structure of human populations and contact patterns, and the stochastic nature of mutation and extinction. In addition, it enables us to compare model output with both phylogenetic and epidemiological data.

We focus on the role of immunity in imposing density-dependent constraints that limit influenza diversity. Influenza antibody recognition tends to decrease with genetic divergence of HA<sub>1</sub>, indicating that cross-protection arising from long-lived memory responses decreases as the sequence divergence between two strains increases (Fig. 2a). In such circumstances, as the antigenic diversity of co-circulating strains increases, so should their mean infection prevalence, thereby increasing production of further variants. If such cross-immunity is the only form of interaction between strains, the expected result of this selection for antigenic novelty is exponential growth of diversity, with concomitant excessive infection incidence as shown in Fig. 2b, c. This diversification can be mitigated by lowering mutation rates and increasing the intensity of cross-immunity (Fig. 2d)—but only at the cost of greatly slowing the

rate of evolution, resulting in unrealistically low fixation probabilities and diversity levels.

More extensive sensitivity analysis, described in detail in the Supplementary Information, suggests that it is impossible to reproduce the observed limited diversity and high fixation rates of influenza A and B without an additional, nonspecific competitive interaction between strains. In particular, we examined the effect of functional constraints on viral evolution in three ways: first, as a crude representation of changes occurring in parts of the viral genome that were not being explicitly modelled, we assumed that every new variant had a random fitness (that is, transmissibility). Second, we explicitly modelled a set of codons that determine viral transmissibility independently from those determining antigenicity. Third, we assumed that there was a transmissibility gradient associated with antigenic space. In each case functional constraints alone are insufficient to explain the limited diversity of influenza.

The primary candidate for a nonspecific competitive interaction between strains is a second immune-response component: short-lived immunity that decays rapidly with time from last exposure and inhibits reinfection by any new strain. Such a response acts as a density-dependent constraint on overall infection incidence, thus limiting effective viral population size and reducing the likelihood of explosive diversity growth.

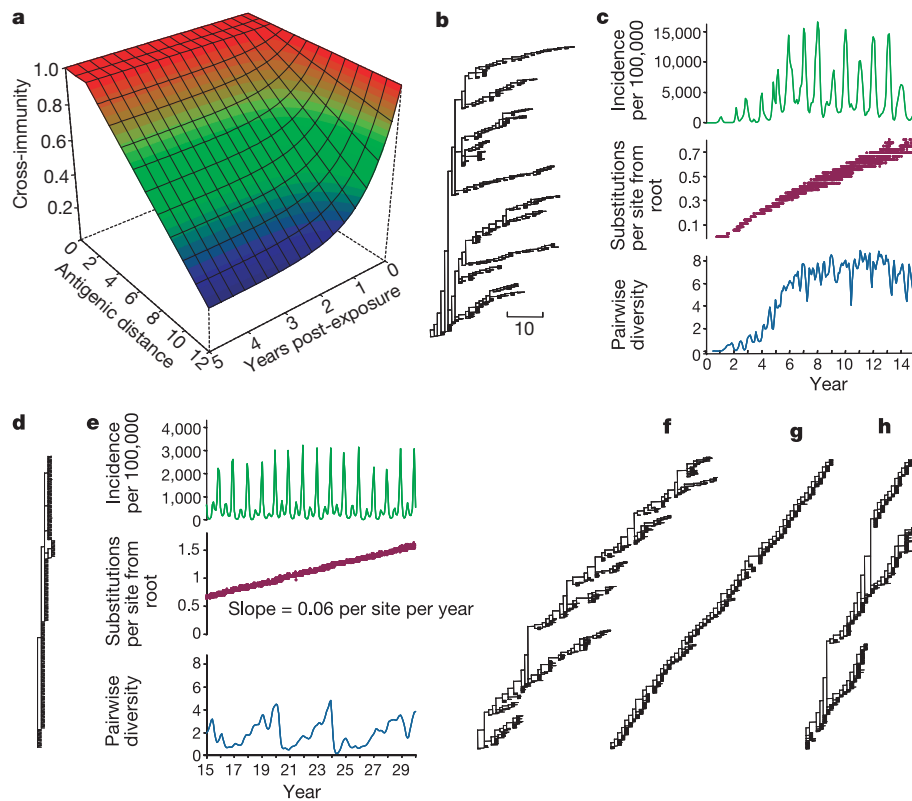


**Figure 2** Model drift dynamics for a single subtype. **a**, Cross-immunity profile assumed for baseline model parameters (see Methods), composed of a long-lived strain-specific memory response and a short-lived nonspecific response. The former gives 99% cross-immunity ( $\theta_1 = 0.99$ ) for strains up to an escape threshold of  $n_t = 2$  changes apart, which drops linearly with increasing genetic distance to a level of  $\theta_0 = 0.25$  for strains with differences at all 12 codons. The latter gives complete protection against reinfection immediately after an infection, but this protection decays exponentially over time with a half-life of six months. **b**, 50-year model tree for baseline parameters but no short-lived nonspecific immunity and mutation rate  $\delta = 10^{-6}$ , showing explosive diversification. For clarity, in every model tree only the 500 strains causing most infections are shown. **c**, 15 years output from model run shown in **b** showing time series of weekly infection incidence in a single geographical patch (upper), the number of nucleotide substitutions

per site (relative to the original strain) for new strains arising through time (middle), and the prevalence-weighted mean pairwise number of amino acid differences between all co-circulating strains (lower)—a measure of diversity. Genetic bottlenecks due to seasonal forcing eventually cause diversity to saturate. **d**, Without short-lived immunity, lowering mutation rate ( $\delta = 2.5 \times 10^{-6}$ ) and/or increasing the immune escape threshold ( $n_t = 4$ ) is only able to achieve constant diversity at the cost of very low fixation rates. **e**, As **c**, but for a model with baseline parameters including short-lived immunity. **f**, 50-year tree from model with baseline parameters including short-lived immunity. **g**, Over-restricted diversity achieved with  $\delta = 10^{-6}$  and  $n_t = 1$ . **h**, Reducing the intensity of cross-immunity (maximum level  $\theta_1 = 0.8$ , minimum level  $\theta_0 = 0.5$ ,  $n_t = 1$ ) and the mutation rate ( $\delta = 2.5 \times 10^{-6}$ ) lowers fixation rate and gives a tree more reminiscent of influenza B.

With the resulting two-component immune memory response (Fig. 2a), our model reproduces key aspects of the dynamics of influenza epidemiology and evolution (Fig. 2e), including the magnitude and seasonality of influenza incidence, a fairly stable viral fixation rate through time<sup>4</sup>, and temporal fluctuations in viral diversity<sup>8</sup> driven by the generation of short-lived viral sublineages and their eventual extinction over the course of several years. Our simulated phylogeny (Fig. 2f) is very similar to the actual pattern of H3 evolution (Fig. 1d). Observed fixation rates can be reproduced at a variety of parameter values (Fig. 2g) by trading off cross-immunity intensity against mutation rates. However, matching both fixation rates and detailed tree shape significantly restricts the space of feasible parameters. Achieving a lower fixation rate and higher level of diversity, such that the resulting tree (Fig. 2h) is more akin to influenza B (Fig. 1c) than to influenza A H3 (Fig. 1a), requires reducing both the intensity of cross-immunity and rate of mutation.

One of the key advantages of our modelling approach is that complete information is provided on the temporal dynamics of both evolution and transmission of all virus variants—information that is difficult to collect from surveillance. Figure 3a illustrates this

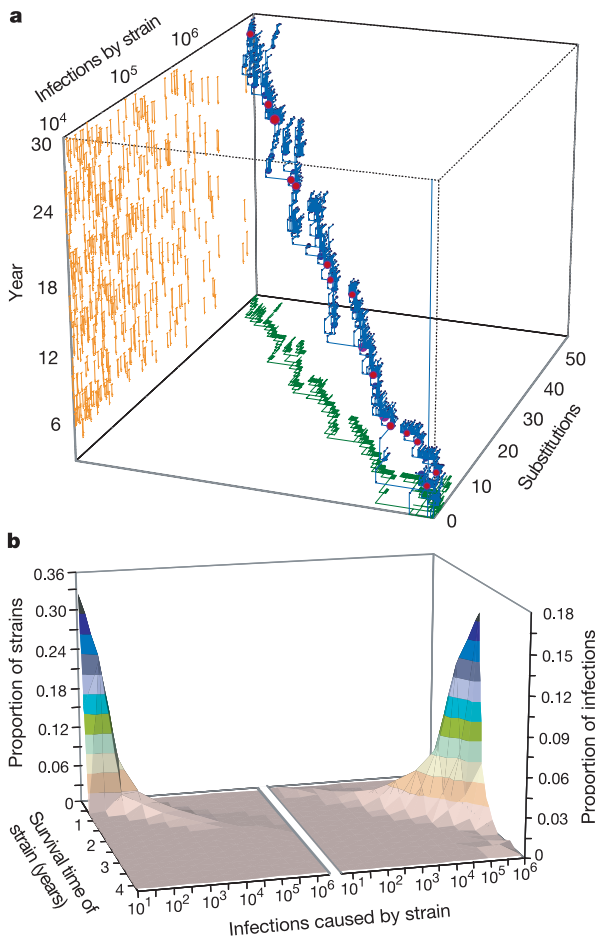


**Figure 3** Detailed evolutionary dynamics of model with short-lived nonspecific immunity. **a**, Three-dimensional tree with genetic distance and time of strain emergence along the y and z axes respectively. The size and colour of internal nodes represent the infection incidence caused by that strain. The traditional two-dimensional phylogenetic tree is projected on the x–z plane. On the y–z plane, each strain causing over 10<sup>4</sup> infections is represented by a line, the start and end of which (along the z axis) indicate time of creation and extinction, and the y-position indicates the total incidence due to that strain. **b**, Joint distribution of strain survival time and log<sub>10</sub> infections caused by each strain. The left pane shows the probability density function calculated for all strains generating over ten infections (averaged over five model realizations), and the right pane the density function for all strains weighted by the number of infections they cause.

point by showing the correlation between genetic distance and time in sequence evolution, and the variability in frequency of different strains. The phylogeny of influenza is seen to arise from multi-strain population dynamics characterized by a highly skewed survival-time distribution for strains (Fig. 3b), where 95% of strains survive for less than a year and infect fewer than 100 people. The less than 1% of strains that successfully become globally established account for 90% of all disease incidence while surviving for 2–3 years. This timescale is consistent with observed survival times of new dominant drift variants<sup>4</sup>.

Two pandemics have occurred since the influenza virus was

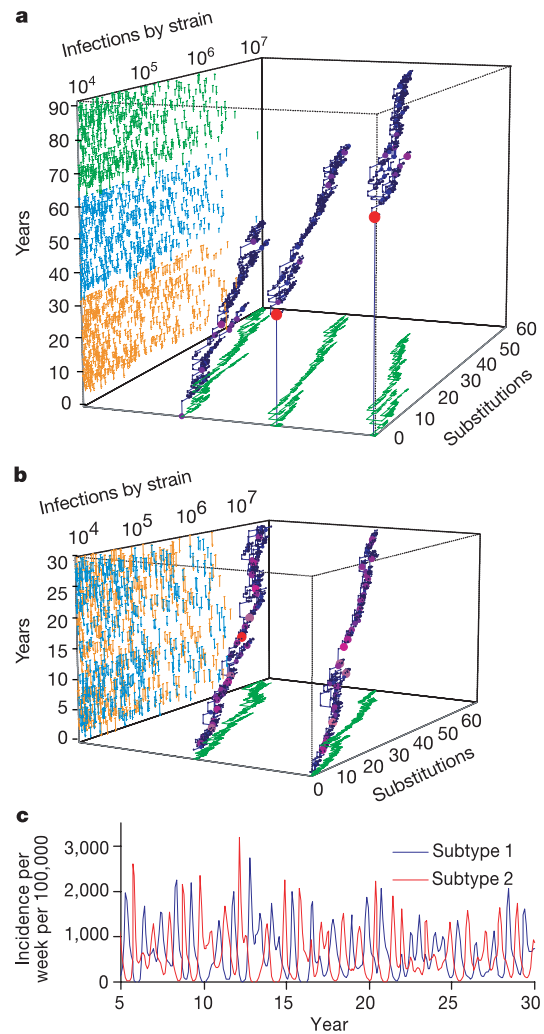


**Figure 4** Model dynamics for interacting subtypes. **a**, Single realization of model with baseline parameters, introducing new subtypes as strains with random genotypes into a single host in the population in years 34 and 64 of a 92-year simulation. Plot shown as Fig. 2c, but three distinct trees can be seen, corresponding to the three pandemic lineages. The strain scatter-plot on the y–z plane is coloured according to subtype. Subtype replacement during pandemics occurred in 100% of the total of 25 model realizations examined. **b**, Subtype coexistence can also occur for these parameter values if the proportions of the host population with immunity to each subtype are close to equilibrium values. The plot shows two subtypes co-evolved from the two-strain equilibrium. **c**, The resulting global incidence time series for co-evolving subtypes predicts that the immunological competition generated by short-lived subtype-transcending immunity would be observable through partial competitive exclusion of different subtypes in sequential years. For **a–c**,  $\tau_{1/2} = 0.1$  years for between-subtype protection and 0.5 years for within-subtype protection. Subtype coexistence is possible, but is an unlikely outcome, if  $\tau_{1/2} = 0.5$  for both within- and between-subtype protection. However, for larger host population sizes, coexistence may become more likely even for that parameter choice.

isolated in 1930. In each case (1957 and 1968) the pandemic strain, an avian–human influenza A reassortant, replaced the previously circulating strain of influenza A. However, coexistence is possible (Fig. 4b) in situations where subtype introduction does not generate a pandemic, as indicated by the current co-circulation of H3 and H1 after the reintroduction of H1 in 1977 into a population with considerable residual herd-immunity against this subtype. The proposed two-component immune response also helps to explain these patterns of competitive exclusion and coexistence between subtypes. Short-lived nonspecific (heterosubtypic) immunity that inhibits immediate reinfection is critical to capture the dynamics of subtype replacement during a pandemic (Fig. 4a).

In the absence of heterosubtypic immunity, the antigenic distance between subtypes generates very limited inter-subtype competition, and subtype elimination becomes unfeasible. With such immunity, subtype extinction becomes highly probable in the context of the globally synchronized large-scale transient dynamics associated with pandemics. However, where subtype introduction causes a smaller epidemic (for example, because of some pre-existing immunity to the new subtype) coexistence is possible if the duration (or effectiveness) of nonspecific immunity is greater within subtypes than between subtypes, a conclusion for which there is abundant empirical evidence<sup>9</sup>. Such immunity gives the less prevalent subtype a frequency-dependent advantage, mitigating the highly unstable dynamics which otherwise rapidly drive the rarer subtype extinct. The resulting incidence time series shows a pattern of fluctuating partial competitive exclusion between subtypes (Fig. 4c), consistent with epidemiological surveillance data (Fig. 1f).

Transient nonspecific immunity is paramount in the generation of such dynamics, and in limiting diversity within subtypes—although other mechanisms that induce nonspecific inter-strain competition (for example, disease-associated reductions in host contact rates) may also contribute. Persistent nonspecific immunity of lower intensity rapidly saturates to affect nearly all hosts and hence fails to impose the intense density-dependent competition that limits viral diversity.

Viral pathogens give unique insight into evolution because their short lifecycle allows dynamical data to be collected at both ecological and evolutionary timescales. Here we show that mathematical models can now give an integrated and detailed description of processes coupling these timescales, reproducing both epidemiological dynamics and patterns of sequence evolution. Thus the influence of epidemiological processes and immunological phenotype on emergent evolutionary dynamics can be explored at a level of realism not previously feasible. Quantitative information on the magnitude of factors determining evolutionary patterns can also be derived (for example, the relationship between *in vitro* haemagglutination assays and the protection afforded against infection with heterologous strains) that would otherwise involve epidemiological and clinical studies of impractically large scale.

Antigenic drift in human influenza has been attributed to step-wise selection for antigenic novelty resulting from an immunity phenotype in which cross-protection declines as the genetic distance between strains increases<sup>10,11</sup>. However, our study shows that without severe density-dependent constraints on the effective population size of the virus, this process alone would lead to rapidly increasing diversity of viral populations. Within a wide range of model variants and parameter ranges explored, transient nonspecific immunity that either prevents rapid reinfection or reduces transmissibility was the only clear candidate for such a constraint. A number of studies support the existence of short-lived nonspecific within-subtype<sup>10–12</sup> and between-subtype<sup>13,14</sup> immune responses, with CTL<sup>15</sup>, natural killer cells<sup>16</sup> and cytokines being proposed effector mechanisms<sup>17</sup>. Quantitative data on the duration of such immunity and its effect on susceptibility or infectiousness is limited, but the timescales of weeks to months explored in this paper are consistent with epidemiological and experimental studies<sup>14,16,18,19</sup>.

Our analysis gives some insight into the potential causes of differences between H1, H3 and B (Fig. 1a–c), as detailed more fully in the Supplementary Information. Alone, the lower fixation rate of H1 and B might simply reflect a lower net mutation rate. However, variation in the levels of genetic diversity between H1, H3 and B may indicate differences in cross-immunity phenotype; that is, reduced maximal cross-immunity, or a lower threshold number of amino acid changes required for evasion of pre-existing immunity. Fuller explanation of differences between influenza viruses circulating within human and other mammalian species<sup>20</sup> will require rigorous analysis of the key loci involved in antigenic selection, together with a more complete model of subtype coevolution. With robust parameterization of population demography and structure, modelling should also give insight into whether the origins of apparent differences are largely ecological (for example, lower population contact rates) or reflect underlying variation in viral phenotype.

Limitations of available quantitative data require models to simplify several aspects of influenza biology and epidemiology<sup>21</sup>. More complete descriptions of antigenicity and other aspects of viral phenotype (such as virulence or transmissibility) will further improve understanding of the constraints on viral evolution. Coupled with more sophisticated representations of spatial heterogeneity in host density and human contact patterns, model correspondence with epidemiological and sequence data will also be enhanced. Collection of such data depends on continued improvement in global surveillance of new influenza strains<sup>22</sup>. Current programmes successfully identify new variants, but the quantitative tracking of strain-specific incidence—although increasingly feasible with the advent of rapid molecular typing methods—remains a long-term objective. This work is essential if statistically predictive modelling is to be achieved, whether applied to predicting new vaccine candidate strains<sup>3,23</sup>, anticipating the effect of increasing population size and vaccine use on viral evolution, or modelling the global spread of future pandemics. □

Methods

Transmission model

Baseline parameter values (selected from the detailed sensitivity analyses described in the Supplementary Information as best reproducing observed patterns of evolution) are given here; parameters used in sensitivity analyses are detailed in the text. We simulate a constant population size of  $N$  (=12 million) hosts, each with lifespan  $L$  (=30 years), equally distributed between  $M$  (=20) geographical patches. The locations of hosts in a patch are randomly distributed with a mean separation of one (in arbitrary units). Each host is labelled by patch index  $p$  ( $1 \leq p \leq M$ ) and host index  $i$  ( $1 \leq i \leq N/M$ ), and at any time is characterized by four variables,  $\{B_{p,i}, T_{p,i}, S_{p,i}, H_{p,i}\}$ , where  $B_{p,i}$  is the time of birth,  $T_{p,i}$  is the time of last infection,  $S_{p,i}$  is the index of the last strain with which the host was infected, and  $H_{p,i}$  characterizes the immune history of the host. Where no prior infection has occurred,  $S = 0$  and  $T = -\infty$ . On infection, hosts are assumed to incubate infection for 2 days (ref. 24), be infectious for the following 4 days (ref. 25), and recover thereafter. Results here assume no co-infection, but are not sensitive to this assumption. Infection and mutation processes were modelled stochastically using a discrete-time model formulation with a one-day time-step. On day  $t$ , the probability a host is exposed to strain  $s$  is given by

$$\rho_{p,i}(t,s) = 1 - \exp \left\{ - [1 + \varepsilon_p \sin(t/365)] \left( \sum_{\substack{i' \in \{S_{p,i'}=s\} \cap \\ \{2 < t - T_{p,i'} \leq 6\} \cap \\ \{r_p(i,i') \leq R\}}} \beta_L + \sum_{\substack{i' \in \{S_{p,i'}=s\} \cap \\ \{2 < t - T_{p,i'} \leq 6\}}} \beta_W \right) - \sum_{p' \neq p} [1 + \frac{1}{2}(\varepsilon_p + \varepsilon_{p'}) \sin(t/365)] \sum_{\substack{i' \in \{S_{p',i'}=s\} \cap \\ \{2 < t - T_{p',i'} \leq 6\}}} \beta_B \right\}$$

where  $r_p(i,i')$  is the distance between hosts  $i$  and  $i'$  in patch  $p$ ,  $R$  (=4) is the threshold distance for local transmission,  $\beta_L$  is the contact rate between hosts in the same spatial locality (defined by  $r_p(i,i') \leq R$ ),  $\beta_W$  is a contact rate representing a less frequent process of mixing between all hosts in a patch, and  $\beta_B$  is the rate of between-patch contacts.  $\beta_B$  and

$\beta_L$  are assigned values to give a basic reproduction number,  $R_0$ , for local transmission in a patch of 5,  $R_0$  for mass-action transmission in a patch of 0.4, and an  $R_0$  of 0.02 between any two patches. Seasonal variation in contact rates is characterized by  $\epsilon_p$ , and is assumed to be opposite in phase for the Northern and Southern hemispheres (represented by setting  $\epsilon_p = +0.25$  for  $1 < p \leq M/2$ , and  $\epsilon_p = -0.25$  for  $M/2 < p \leq M$ ).

The probability that a host is infected upon exposure depends on the strain  $s$ , and the host's immune history. Each strain is characterized by  $A$  epitopes, each consisting of  $C$  codons (three nucleotide bases). Immunity is assumed to be specific to the set of amino acids to which the host has been exposed at each codon, and for simplicity, no functional constraints are imposed on the amino acid sequences. For the default values of  $A = 4$  and  $C = 3$  used here, a total of  $4 \times 10^{15}$  strains are possible. Antigenic distance,  $d(s,H)$  between a strain  $s$  and the immune history of a host,  $H$ , is then simply defined as the number of codons in strain  $s$  for which the amino acid has not been previously encountered by the host. The level of cross-protection from infection provided at a certain antigenic distance is given by the function  $f(d)$ , where we assume  $f(d) = \theta_1 + (\theta_0 - \theta_1)(d - n_t)/(AC - n_t)$  for  $d \geq n_t$ ,  $f(d) = \theta_1$  for  $0 < d < n_t$ , and  $f(d) = 1$  for  $d = 0$ .  $n_t (=2)$  is the threshold level of change necessary for cross-protection to drop below the maximal level set by  $\theta_1 (=0.99)$ , and  $\theta_0 (=0.25)$  is the minimal level of cross-protection mounted against a strain with no similarity to a previously encountered strain at the codons modelled ( $=0$  for no cross-protection). These assumptions reflect empirical studies suggesting that two or more substitutions at key antigenic sites are required to escape pre-existing immunity<sup>26,27</sup>.

The probability that a host will be infected by a strain following exposure is given by

$$\varphi_{p,i}(t,s) = \{1 - \omega \exp[-(t - T_{p,i})/\tau]\} [1 - f[d(s,H_{p,i})]]$$

where  $\tau (=270$  days) is the decay timescale (half-life =  $\tau_{1/2} = 187$  days  $\approx 6$  months) and  $\omega (=1)$  is the peak level ( $0 \leq \omega \leq 1$ ) of a short-lived strain-transcending immune response that protects against reinfection in the weeks after an infection (see main text). If a host is infected following exposure, its immune history is updated to include the new strain. If exposure does not result in infection, we assume that no immune response is raised to the new strain but that pre-existing immune responses are boosted (akin to the 'original antigenic sin' response<sup>28</sup>), by resetting  $T_{p,i}$  to  $t - 6$  immediately after exposure.

There is a probability  $\delta (=10^{-5})$  per base per day that a nucleotide substitution will occur in the virus in an infected host and the resulting mutant strain will replace the pre-existing strain in that individual. The individual is then infectious with the new strain. All strains are assumed to have the same intrinsic transmissibility (but see Supplementary Information), and model runs were started from near the single-strain equilibrium.

Received 18 November 2002; accepted 21 February 2003; doi:10.1038/nature01509.

1. Webster, R. G., Bean, W. J., Gorman, O. T., Chambers, T. M. & Kawaoka, Y. Evolution and ecology of influenza A viruses. *Microbiol. Rev.* **56**, 152–179 (1992).
2. Bush, R. M., Fitch, W. M., Bender, C. A. & Cox, N. J. Positive selection on the H3 hemagglutinin gene of human influenza virus A. *Mol. Biol. Evol.* **16**, 1457–1465 (1999).
3. Cox, N. *et al.* in *Options for the Control of Influenza II* (eds Hannoun, C., Kendal, A. P., Klenk, H. D. & Ruben, F. L.) 223–230 (Elsevier Science, Amsterdam, 1993).
4. Fitch, W. M., Bush, R. M., Bender, C. A. & Cox, N. J. Long term trends in the evolution of H(3) H3A1 human influenza type A. *Proc. Natl Acad. Sci. USA* **94**, 7712–7718 (1997).
5. Lindstrom, S. E. *et al.* Comparative analysis of evolutionary mechanisms of the hemagglutinin and three internal protein genes of influenza B virus: multiple cocirculating lineages and frequent reassortment of the NP, M, and NS genes. *J. Virol.* **73**, 4413–4426 (1999).
6. Daly, J., Wood, J. & Robertson, J. in *Textbook of Influenza* (eds Nicholson, K., Webster, R. & Hay, A.) 168–177 (Blackwell Science, Oxford, 1998).
7. Bush, R. M., Bender, C. A., Subbarao, K., Cox, N. J. & Fitch, W. M. Predicting the evolution of human influenza A. *Science* **286**, 1921–1925 (1999).
8. Cox, N. & Regnery, H. in *Options for the Control of Influenza III* (eds Brown, L. E., Hampson, Q. W. & Webster, R. G.) 591–598 (Elsevier Science, Amsterdam, 1996).
9. Glezen, W. P. & Couch, R. B. in *Viral Infections of Humans* (eds Evans, A. S. & Kaslow, R. A.) 473–505 (Plenum Medical, New York, 1997).
10. Gill, P. W. & Murphy, A. M. Naturally acquired immunity to influenza type A. A further prospective study. *Med. J. Aust.* **2**, 761–765 (1977).
11. Frank, A. L., Taber, L. H. & Porter, C. M. Influenza B virus reinfection. *Am. J. Epidemiol.* **125**, 576–586 (1987).
12. Frank, A. L. & Taber, L. H. Variation in frequency of natural reinfection with influenza A viruses. *J. Med. Virol.* **12**, 17–23 (1983).
13. Yetter, R. A., Lehrer, S., Ramphal, R. & Small, P. A. Outcome of influenza infection: effect of site of initial infection and heterotypic immunity. *Infect. Immun.* **29**, 654–662 (1980).
14. Sonoguchi, T., Naito, H., Hara, M., Takeuchi, Y. & Fukumi, H. Cross-subtype protection in humans during sequential, overlapping, and/or concurrent epidemics caused by H3N2 and H1N1 influenza viruses. *J. Infect. Dis.* **151**, 81–88 (1985).
15. Yewdell, J. W., Bennink, J., Smith, G. L. & Moss, B. Influenza A virus nucleoprotein is a major target antigen for crossreactive anti-influenza A virus cytotoxic T lymphocytes. *Proc. Natl Acad. Sci. USA* **82**, 1785–1789 (1985).
16. Skoner, D. P. *et al.* Effect of influenza A virus infection on natural and adaptive cellular immunity. *Clin. Immunol. Immunopathol.* **79**, 294–302 (1996).
17. Seo, S. H., Peiris, M. & Webster, R. G. Protective cross-reactive cellular immunity to lethal A/Goose/Guangdong/1/96-like H5N1 influenza virus is correlated with the proportion of pulmonary CD8(+) T cells expressing gamma interferon. *J. Virol.* **76**, 4886–4890 (2002).
18. Sambhara, S. *et al.* Heterosubtypic immunity against human influenza A viruses, including recently emergent avian H5 and H9, induced by FLU-ISCOM vaccine in mice requires both cytotoxic T-lymphocyte and macrophage function. *Cell Immunol.* **211**, 143–153 (2001).
19. McElhane, J. E., Meneilly, G. S., Pinkoski, M. J., Lechelt, K. E. & Blackley, R. C. Vaccine-related determinants of the interleukin-2 response to influenza vaccination in healthy young and elderly adults. *Vaccine* **13**, 6–10 (1995).
20. Nicholson, K. G., Webster, R. G. & Hay, A. J. *Textbook of Influenza* (Blackwell Science, Oxford, 1998).

21. Earn, D. J., Dushoff, J. & Levin, S. A. Ecology and evolution of the flu. *Trends Ecol. Evol.* **17**, 334–340 (2002).
22. Layne, S. P. *et al.* A global lab against influenza. *Science* **293**, 1729 (2001).
23. Bush, R. M., Bender, C. A., Subbarao, K., Cox, N. J. & Fitch, W. M. Predicting the evolution of human influenza A. *Science* **286**, 1921–1925 (1999).
24. Moser, M. R. *et al.* An outbreak of influenza aboard a commercial airliner. *Am. J. Epidemiol.* **110**, 1–6 (1979).
25. Benenson, A. S. *Control of Communicable Diseases in Man* (American Public Health Association, Washington DC, 1975).
26. Wilson, I. A. & Cox, N. J. Structural basis of immune recognition of influenza virus hemagglutinin. *Annu. Rev. Immunol.* **8**, 737–771 (1990).
27. Smith, C. B., Cox, N. J., Subbarao, K., Taber, L. H. & Glezen, W. P. Molecular epidemiology of influenza A(H3N2) virus reinfections. *J. Infect. Dis.* **185**, 980–985 (2002).
28. Hoskins, T. W., Davies, J. R., Smith, A. J., Miller, C. L. & Allchin, A. Assessment of inactivated influenza-A vaccine after three outbreaks of influenza A at Christ's Hospital. *Lancet* **1**, 33–35 (1979).
29. Swofford, D. L. *PAUP\*: Phylogenetic Analysis Using Parsimony* (Sinauer, Sunderland, 1998).
30. Morbidity and Mortality Weekly Reports (Centers for Disease Control and Prevention, annual reports on influenza frequency, 1986–2002).

Supplementary Information accompanies the paper on Nature's website (<http://www.nature.com/nature>).

**Acknowledgements** We thank N. J. Cox for discussions. N.M.F. thanks the Royal Society, Howard Hughes Medical Institute and Medical Research Council, A.P.G. thanks the Miller Institute, and R.M.B. thanks the NIH for research funding.

**Competing interests statement** The authors declare that they have no competing financial interests.

**Correspondence** and requests for materials should be addressed to N.M.F. (e-mail: neil.ferguson@ic.ac.uk).

## Unravelling angiosperm genome evolution by phylogenetic analysis of chromosomal duplication events

John E. Bowers\*, Brad A. Chapman\*, Junkang Rong & Andrew H. Paterson

Plant Genome Mapping Laboratory, University of Georgia, Athens, Georgia 30602, USA

\* These authors contributed equally to this work

Conservation of gene order in vertebrates is evident after hundreds of millions of years of divergence<sup>1,2</sup>, but comparisons of the *Arabidopsis thaliana* sequence<sup>3</sup> to partial gene orders of other angiosperms (flowering plants) sharing common ancestry ~170–235 million years ago<sup>4</sup> yield conflicting results<sup>5–11</sup>. This difference may be largely due to the propensity of angiosperms to undergo chromosomal duplication ('polyploidization') and subsequent gene loss<sup>12</sup> ('diploidization'); these evolutionary mechanisms have profound consequences for comparative biology. Here we integrate a phylogenetic approach (relating chromosomal duplications to the tree of life) with a genomic approach (mitigating information lost to diploidization) to show that a genome-wide duplication<sup>3,13–17</sup> post-dates the divergence of *Arabidopsis* from most dicots. We also show that an inferred ancestral gene order for *Arabidopsis* reveals more synteny with other dicots (exemplified by cotton), and that additional, more ancient duplication events affect more distant taxonomic comparisons. By using partial sequence data for many diverse taxa to better relate the evolutionary history of completely sequenced genomes to the tree of life, we foster comparative approaches to the study of genome organization, consequences of polyploidy, and the molecular basis of quantitative traits.

Angiosperms sustain humanity by providing oxygen, medicines, food, feed, fibre, fuel, erosion and flooding control, soil regener-

